FULL PAPER

Enhancing Output Power of Cylindrical Triboelectric Nanogenerators by Segmentation Design and Multilayer Integration

Wei Tang, Chi Zhang, Chang Bao Han, and Zhong Lin Wang*

The triboelectric nanogenerator (TENG) is a newly invented technology that is effective for harvesting ambient mechanical energy for portable electronics, self-powered sensor networks, etc. Here, by introducing segmentation and multilayer integration into the cylindrical TENG, the generator's output is enhanced significantly. With a four-layer and thirty-segment configuration, the TENG produces a short-circuit current of 86 μA (13.5 μA m^{-2}) and power of 4.3 mW (676 mW m^{-2}) at a rotating speed of 600 rpm, which are respectively over 70 and 15 times higher than those of the one-layer and one-segment structure. This makes the TENG a sufficient power supply for conventional electronics, such as light bulbs and temperature sensors. Furthermore, it is demonstrated that the segmentation design is a perfect self-power management technique to automatically lower the TENG's output voltage and increase its output current without scarifying the output power. The fractal geometry is an effective way to maximize the TENG's contact surface area and thereby the output performance.

1. Introduction

With the rapid increasing of portable electronics and wireless sensing networks, scavenging ambient mechanical energy as a sustainable power source for powering these devices is a focus of today's research. Various approaches based on piezoelectric,[1–4] electromagnetic,[5,6] electrostatic effects[7,8] have been demonstrated for harvesting mechanical energy In the last few years, combining triboelectric effect and the electrostatic induction phenomenon, triboelectric nanogenerater (TENG) is newly invented, showing a significantly high power output and a high energy conversion efficiency up to 50%.[9–21] Therefore, it enables self-powered, autonomous electronics and potentially large-scale power generation possible.[10,14] Unlike the traditional electromagnetic induction generator (EMIC), the TENG

is equivalent to a current source where the current depends significantly on the induced charge amount and the charging/discharging rate.[22] Considering that, the cylindrical TENG was selected to be optimized in this work by employing multilayer integration and segmentation. It was found that when the layer number is four, the segmental number is thirty, and the rotating speed is 600 rpm, the TENG's output current and power reached 86 μA (13.5 μA m^{-2}) and 4.3 mW (676 mW m^{-2}), which are 70 and 15 times higher than those of the one-layer and one-segmented TENG. The TENG has been applied to drive multiple light-emitting diodes (LEDs) and a temperature sensor. As a general conclusion, our work implies that the segmentation is an ideal self-power-managing technique for TENGs, and the fractal geometry is an effective way to enlarge their contact surface area and thus the output performance.

2. Experiments

The basic structure of the cylindrical TENG with two segmentation units and four layers integration is shown in **Figure 1**a. It mainly consists of two series of coaxial complementary petals. Aluminum (Al) was selected as both the structural and the electrode material due to its good mechanical strength and conductivity. As for the fabrication, the two-sector-structured disk-shaped substrate with a diameter of 9 cm (63.58 cm^2 in area), was first processed by mechanical cutting from an Al plate, leaving quarter-annulus slits for petals. Petal series with a thickness of 3 mm for each petal were fabricated by the same way. Since polytetrafluoroethylene (PTFE) possesses a large difference in electron attracting ability with respect to Al, 30 μm-thick PTFE was tailored and securely attached to the surfaces of one petal series. Afterwards, petals were assembled into their related coaxial disks (the tight contact also ensured the electric connection). Therefore, the PTFE-covered petals and Al petals were brought to a face-to-face immediate contact with contacting surface area of 72.8 cm^2, and the PTFE side was driven to spin anticlockwise around their common axis. To promote the triboelectrification and

W. Tang, C. Zhang, C. B. Han, Prof. Z. L. Wang
Beijing Institute of Nanoenergy and Nanosystems
Chinese Academy of Sciences
Beijing 100083, China
Prof. Z. L. Wang
School of Material Science and Engineering
Georgia Institute of Technology
Atlanta, GA 30332, USA
E-mail: zlwang@gatech.edu

www.MaterialsViews.com

ADVANCED
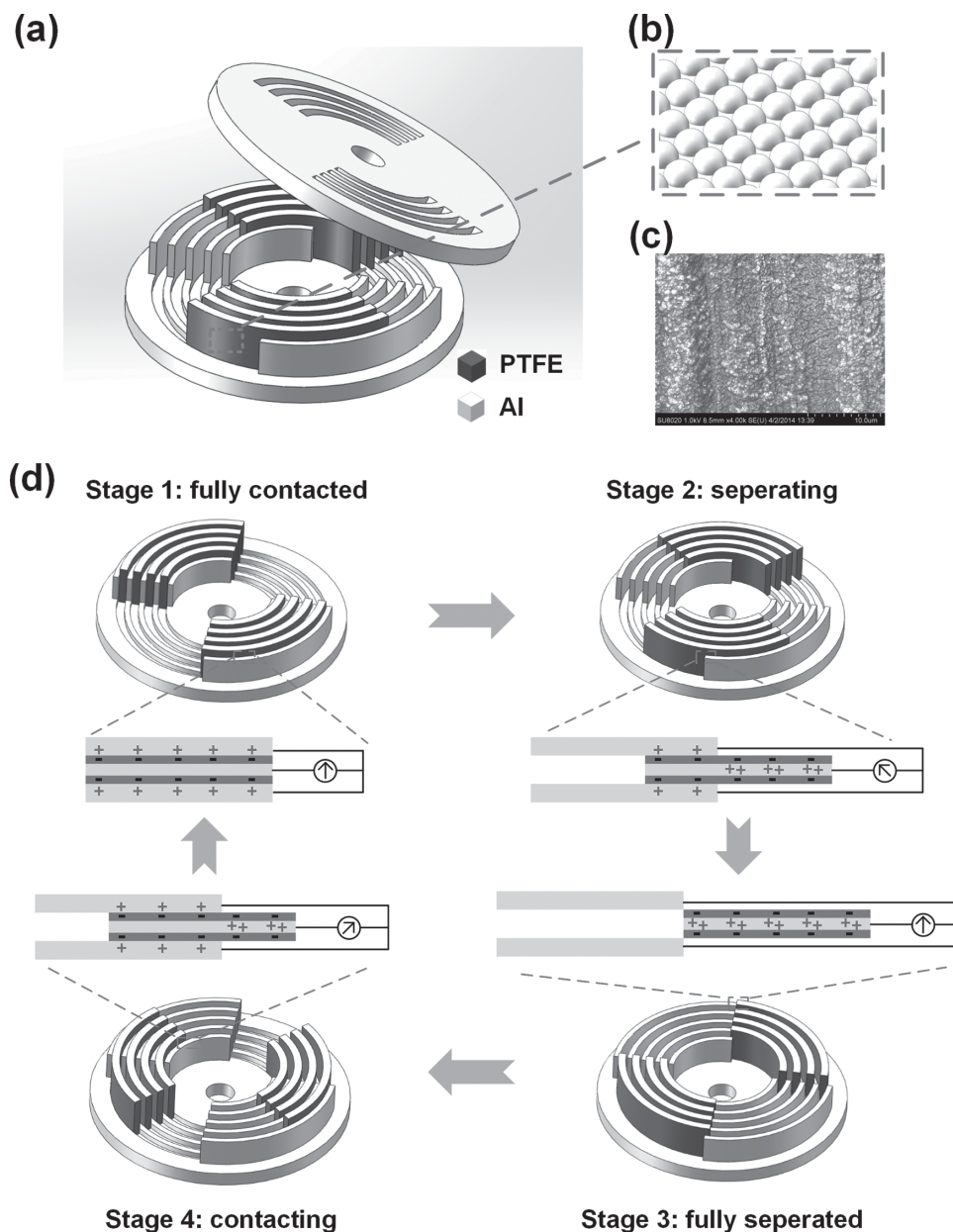FUNCTIONAL
MATERIALS
www.afm-journal.de

FULL PAPER

Figure 1. Basic structure and proposed working principle of the cylindrical TENG. a) A schematic illustration showing the structure design of the TENG. b) The PTFE nanohemisphere array created on the surface area. c) A top-view SEM image of the PTFE nanohemisphere array showing its uniformity in a large range. d) Schematic illustrations showing the proposed working principle of the TENG with the electrons flow diagram in four consecutive stages within a full cycle of electricity generation.

increase the effective contact area between the two sliding materials, a PTFE nanohemisphere (NHS) array was created on the PTFE surface by a top-down approach through plasma etching in argon (Ar) and oxygen (O_2) (PVA ION 40 GAS PLASMA SYSTEM), as displayed in the Figure 1b. Scanning electron microscopy (SEM) images of the PTFE NHSs are shown in Figure 1c. After 20-min of etching, the NHSs with an average diameter of 500 nm were uniformly distributed on the surface of PTFE film. Figure S1 (Supporting Information) shows the SEM picture of the nanopatterned PTFE after 30 000 working cycles.

The working principle of this configuration of cylindrical TENG is based on the triboelectrification and the relative-rotation-induced along-cylinder charge separation between Al and PTFE, as shown in Figure 1d. In the relative rotation, the PTFE surface and Al surface slide against each other, so that the electrons will be injected from the Al petals to the surface of the PTFE film, leaving net positive charges on the Al petals and net negative charges on the PTFE petals. The TENG's electricity generation process can be divided into four stages: in Stage 1, Al and PTFE petals are at an overlapping position. Since the two charged surfaces are
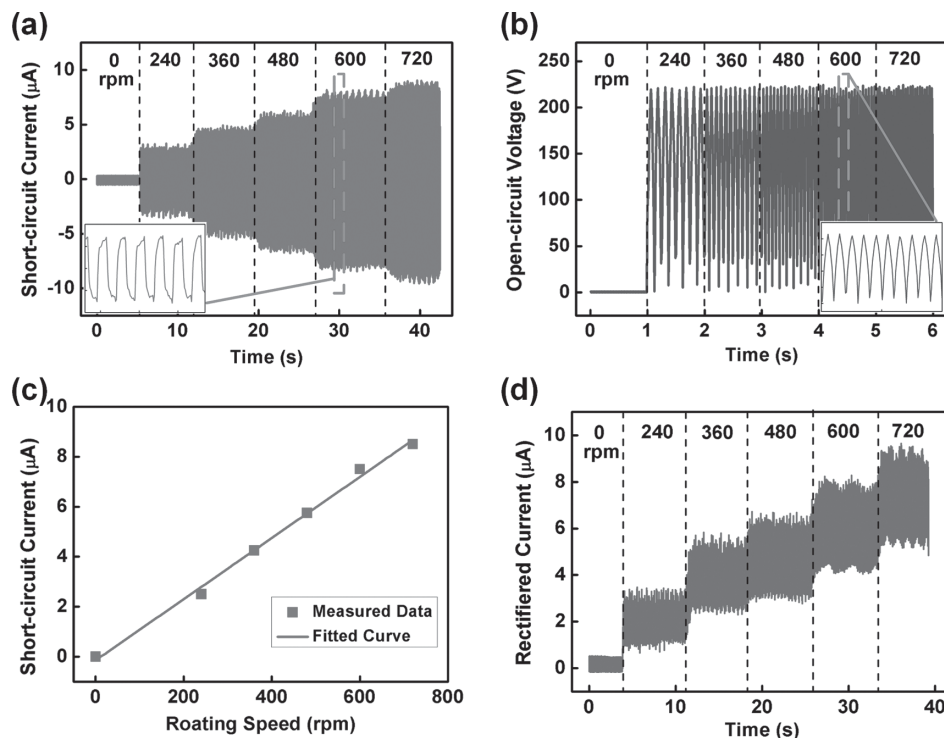
ADVANCED
FUNCTIONAL
MATERIALS
www.afm-journal.de

Materials Views
www.MaterialsViews.com

Figure 2. Results of electric measurements for the cylindrical TENG having a petal number of four and a segmentation number of two. a) Short-circuit current (I_{sc}) at variable rotation speed. b) Open-circuit voltage (V_{oc}) at variable rotation speed. c) Current peak as a function of the rotating speed. d) Rectified current at variable rotation speed.

closely contacted with each other so that there is little polarization, there will be no potential difference between the two electrodes, thus no current flow in the external load. When the PTFE part rotates in reference to the Al part, the corresponding two segments start to have a partially mismatched contact area (Stage 2), and the tribo-charges are thus separated in the direction almost parallel to the sliding direction, which will induce a higher potential on the Al petals than on the PTFE's electrodes; thus the electrons in the electrode surrounded by the PTFE film will be driven to flow to the Al petals through an external circuit (forming a current flow as shown in Figure 1d Stage 2), so that an opposite potential is generated to balance the potential difference created by the separated tribo-charges. In this process, the electrons keep flowing until the two parts reach fully mismatch in the contacting segmented areas (e.g., 90° of rotation in this case), which is represented by Stage 3. At this moment, both the induced potential difference and the amount of transferred charges between the two electrodes reach the maximum values. In Stage 4 as the top plate continues spinning, the PTFE petals begins to get contacted with another adjacent sector of Al petals, and the potential difference between the two electrodes will drop with the decrease of the mismatched area. As a result, the electrons will flow back in the opposite direction from the Al petals to the electrode attached to the PTFE film. Thus, the entire process will result in an alternating-current (AC) output. Such a charge transfer cycle will start over from Stage 1 when the two plates reach a complete overlapping again.

According to our previous research,[11] the absolute value of the short-circuit current I_{sc} between the two electrodes is determined by:

$$|I| = \frac{\Delta Q}{\Delta t} = \frac{\sigma S}{\theta} \omega = 2\pi \frac{\sigma S(m)}{\theta} \frac{n}{60} = \sigma S(m) \frac{nl}{30} \quad (1)$$

where σ is a constant value of triboelectric charge density, θ is one sector's angle, l is the segmentation number, S is the contacting area of two series of petals, which is a function of the petals' layer number m, and n is the rotating speed in a unit of rounds per minute (rpm). It implies that the TENG's segmentation and layer integration play important roles on its output performance. **Figure 2**a,b show the measured short-circuit current and open-circuit voltage of a TENG, in which the petals' layer number is four and the segmentation number is two, and the rotating speed ranged from 0 to 720 rpm. The enlarged views in the insets exhibit the continuous AC signal at 600 rpm. The output current is enhanced with higher rotating speed and the good linear fitting in Figure 2c is coherently consistent to Equation (1). The output voltage is nearly independent of the rotating speed, correlating with the previous work.[11] Additionally, Figure 2d shows the device's current after rectification, which is similar to a direct-current (DC) signal.

As discussed above, the petals' layer number m has a significant influence on the TENG's output. In this regard, we studied the TENG with different layer integration (**Figure 3**a). I_{sc} and V_{oc} measurement were carried out to demonstrate the effect of this configuration on the output performance. Experiment results
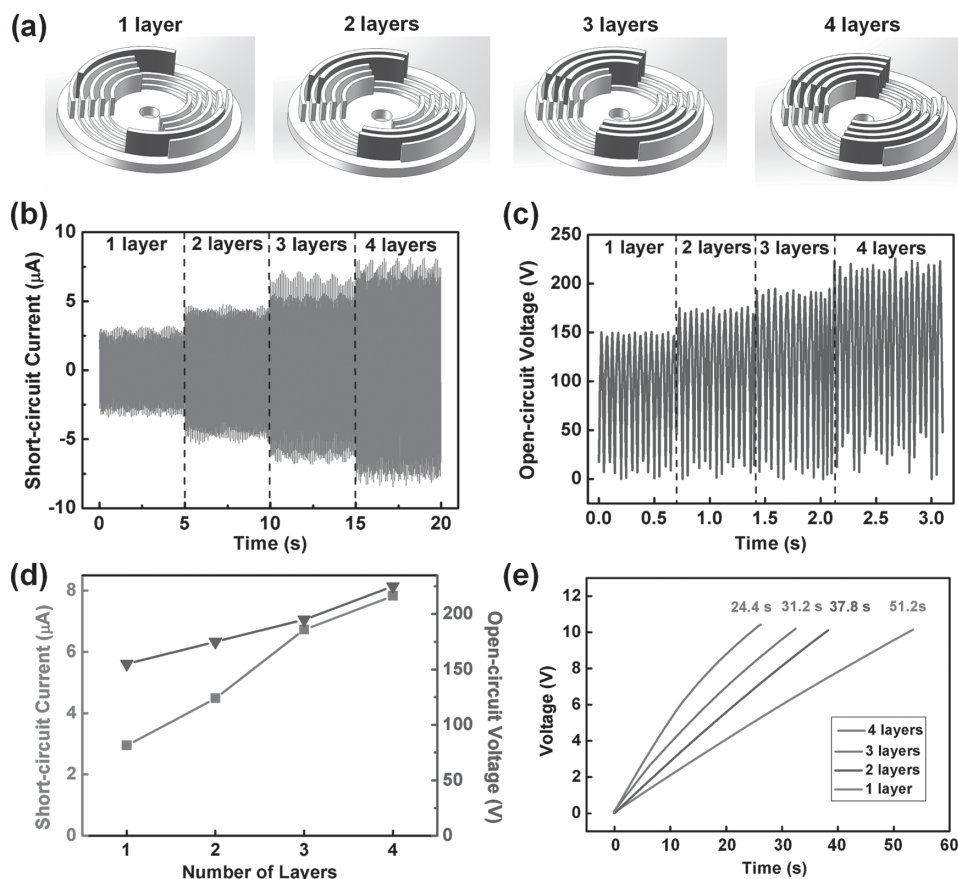
www.MaterialsViews.com

ADVANCED
FUNCTIONAL
MATERIALS
www.afm-journal.de

FULL PAPER

Figure 3. a) Configurations of various petal numbers of TENGs. b,c) I_{sc} and V_{oc} of various petal numbers of TENGs. d) I_{sc} and V_{oc} as a function of the petal number. e) Capacitor charging measurement of various petal numbers of TENGs.

show this trend clearly (Figure 3b,c). As the petal's number increased from 1 to 4, I_{sc} increased from 3 µA to 7.5 µA, while V_{oc} increased from 150 V to 225 V slightly. The increase of I_{sc} was owing to the enlargement of the friction surface area. Since the added layer possessed smaller area than the first layer did, the increasing slope decreased accordingly. As for the open-circuit voltage, it increased due to the increase of the generated tribo-charges. Likewise, with the layer number become bigger, the TENG showed an enhancement in the capacitor charging, as shown in Figure 3d. The charged capacitor is 10 µF, and the TENG with the four-layer integration configuration took 24.4 s, which was two times shorter than the one-layer TENG, to charge the capacitor up to 10 V.

It can be found from the above experiments that the tribo-electric nanogenerator is a surface effect dominated device. The bigger the friction surface area is, the larger the output current and voltage are. Compared to the previous disk and cylindrical TENGs,[11,20] this TENG expands the friction surface into a 3D space. This concept could be suitable for all kinds of TENGs. Moreover, it can be further improved according to the well-known fractal geometry. **Figure 4** exhibits this principle, and related configurations and measurements. The first column stands for the original in-plane TENG configuration. It output a current of 2 µA and charges of 122.3 nC. Next column stands for the TENG in this work or any other multilayered

TENG. By introducing more contact surface while keeping the volume constant, the TENG enhanced the output current up to 7.2 µA and charges to 339.1 nC. In addition, by the self-similar construction rule, the third-order TENG is shown in the right column. Likewise, due to the increase of the frication surface, this TENG further enhanced the output current and charges up to 11 µA and 607.8 nC, which are over five times larger than that of the planar TENG. Inferably, when the order becomes higher, the TENG will feature in much more surface area and therefore much larger output.

Except the layer integration, the I_{sc} will increase linearly with the segmentation number l, according to the theoretical analysis. To verify this relationship, a group of electrical measurements were performed with variable segmentation number assembled on the four-layer cylindrical TENG, which is presented in **Figure 5**a. Figure 5b,c show the measured short-circuit current and open-circuit voltage with different segmentation number. As expected, the I_{sc} was largely enhanced from 3.7 µA to 86 µA when the segmentation number increased from 1 to 30, and the linear relationship is shown in Figure 5d, coherently consistent with the behavior predicted by Equation (1). The obvious enhancement can also be seen from the capacitor charging measurement (Figure 5e). On the other hand, the open-circuit voltage decreased with the increasing segmentation number (Figure 5c,d). The decay of V_{oc} might
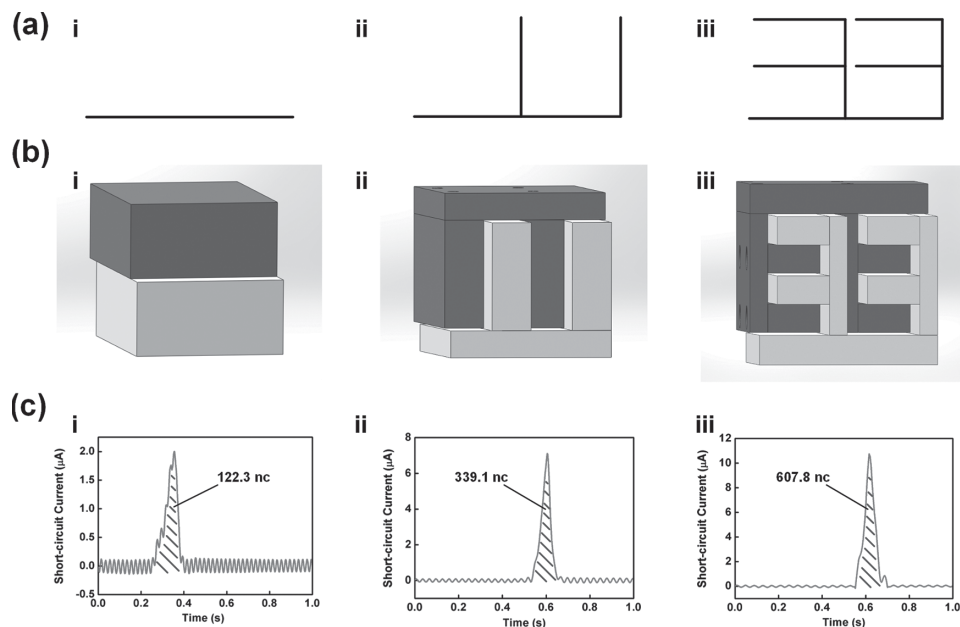
Figure 4. a) Sketches of the fractal construction rule for TENGs. b) Configurations of three orders of TENGs. c) Current and charges measurements of three orders of TENGs.
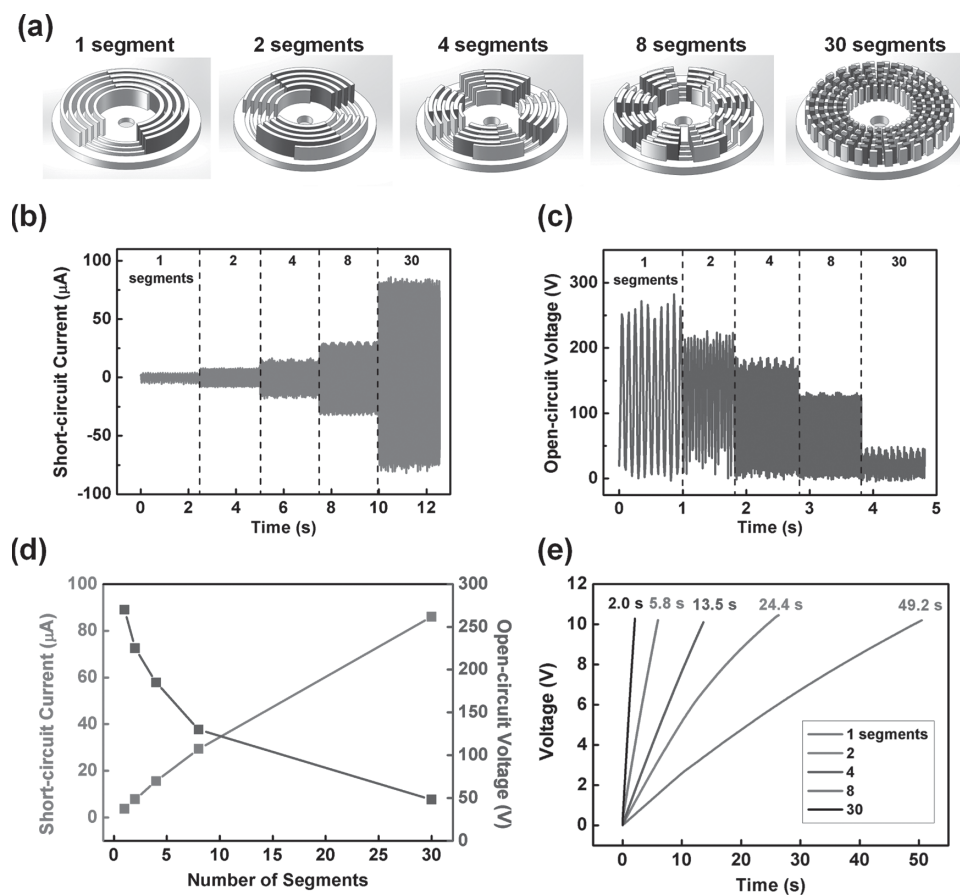

Figure 5. a) Configurations of various segmentation numbers of TENGs. b,c) I_{sc} and V_{oc} of various segmentation numbers of TENGs. d) I_{sc} and V_{oc} as a function of the segmentation number. e) Capacitor charging measurement of various segmentation numbers of TENGs.

Materials Views
www.MaterialsViews.com

ADVANCED
FUNCTIONAL
MATERIALS
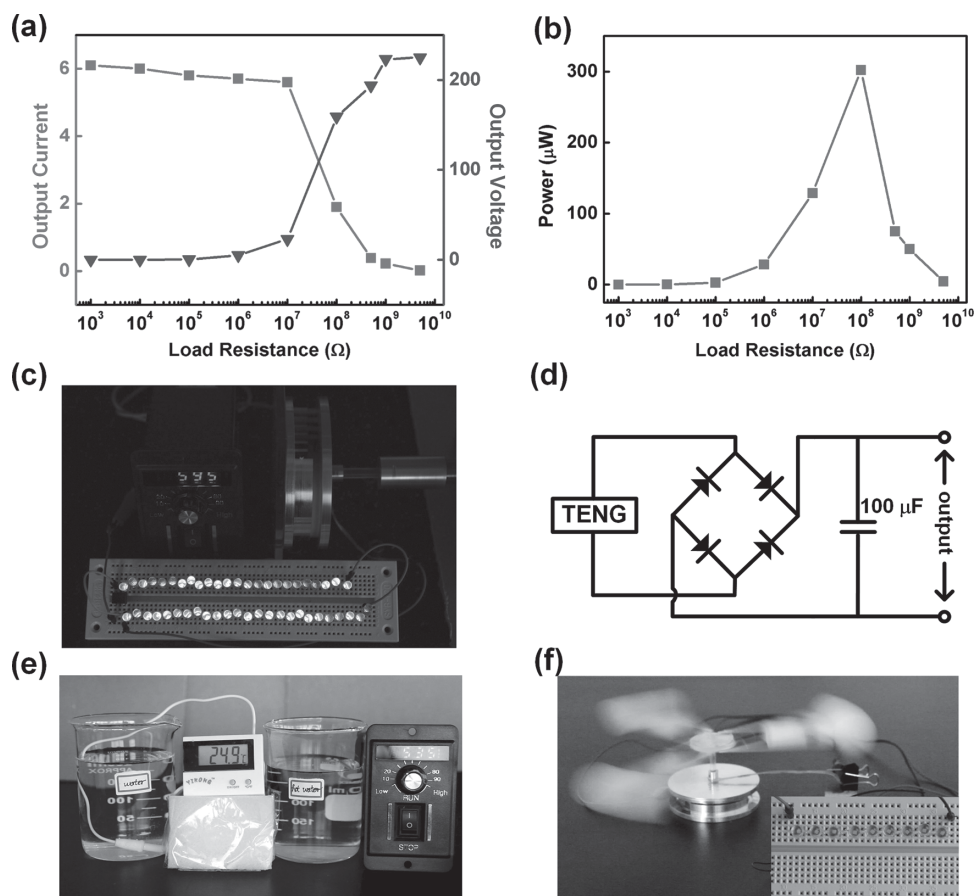www.afm-journal.de

FULL PAPER

Figure 6. a,b) Load matching test at a rotating speed of 600 rpm. c) The demonstration of the TENG as a direct power source for LED bulbs. d) A circuit diagram applied for the commercial electronics. e) The temperature measurement performed by a commercial temperature sensor, driven by the rotating TENG. f) A demonstration of the TENG for harvesting ambient energy.

be attributing to a significant increase in the side capacitance between the two cylinder petal series, which was predicted in the previous work.[21,23] Our FEA analysis also shows this descending trend with respect to the increasing segmentation number. As the positive and negative charges distribute more dispersed, the electric potential difference gets lower (Figure S2, Supporting Information). This demonstration implies a self-power-managing triboelectric nanogenerator, which means the segmentation configuration will lower the TENG's voltage and increase its output current without an external transformer.

For different practical applications, the generator is usually applied on external loads with variable resistances, so that the output will deviate from the short circuit or open circuit conditions. In this regard, the output performance of the TENG was systematically studied at different loads. **Figure 6**a shows the resistance dependence of both output current and voltage, from 1 KΩ to 10 GΩ. The output current decreased with the increasing resistance while the output voltage show a reverse trend, but both the current and voltage tend to saturate at both high and low ends of the resistance. Additionally, Figure 6b shows the related power output at various resistances. To further demonstrate the ability of the TENG as a direct power source for electronics, about 50 commercial LED bulbs were

utilized as external loads. As illustrated in Figure 6c, at the rotating speed of 595 rpm, all of the LED bulbs were continuously lighted up (Video S1 in the Supporting Information). Subsequently, a commercial temperature meter was connected with the TENG through the circuit diagram in Figure 6d. At the rotating speed around 535 rpm, the temperature meter was powered up and performed sustainably (Video S2, Supporting Information). In addition to being driven by an electric motor, the TENG was further tested in normal environment where the wind energy was harvested. As shown in Figure 6f, the TENG was driven by a moderate breeze with the wind speed of 7 m s^{-1}, and it was able to light up ten LED bulbs (Video S3, Supporting Information).

3. Conclusions

In summary, we have demonstrated a design for a cylindrical rotating TENG with multiple layer integration and segmentation based on the sliding electrification. It was further found that the segmentation configuration is an ideal self-power managemeng technique to lower the TENG's output voltage but increase its current without sacrificing the output power, and the fractal geometry is an effective way to maximize its

contact surface area and thus the output performance. Specifically, a cylindrical TENG with four petal layers and 30 segmentation units could achieve short-circuit current of 86 µA (13.5 µA m^{-2}) and power of 4.3 mW (676 mW m^{-2}) at a rotating speed of 600 rpm, which were respectively over 70 and 15 times higher than those of the one-layer and one-segmented TENG. Thereby, it can be used as a direct power source for powering about 50 LED bulbs in real time as well as a commercial temperature meter. Furthermore, driven by a moderate breeze with a wind speed of 7 m s^{-1}, the TENG was able to light 10 LEDs. This study demonstrates the possibility to effectively harvest mechanical energy from rotational motion through 3D integration using TENGs. It also can be used to design active sensors for monitoring rotational motion and speed. The TENGs can be further applied in many environments to harvest energy from air and water flow as a sustainable power supply for outdoor sensors, which will open a wide range of applications, such as self-powered environmental sensors and wildlife tracking devices.

Supporting Information

Supporting Information is available from the Wiley Online Library or from the author.

Acknowledgements

[1] Z. L. Wang, J. Song, *Science* **2006**, *312*, 242.
[2] R. Yang, Y. Qin, L. Dai, Z. Wang, *Nat. Nanotechnol.* **2008**, *4*, 34.
[3] S. Xu, Y. Qin, C. Xu, Y. Wei, R. Yang, Z. L. Wang, *Nat. Nanotechnol.* **2010**, *5*, 366.
[4] C. Chang, V. Tran, J. Wang, Y. Fuh, L. Lin, *Nano Lett.* **2010**, *10*, 729.
[5] S. Beeby, R. Torah, *J. Micromech. Microeng.* **2007**, *17*, 1257.
[6] P. Glynne-Jones, M. Tudor, *Sens. Actuators A* **2004**, *110*, 344.
[7] P. Mitcheson, P. Miao, B. Stark, *Sens. Actuators A* **2004**, *115*, 523.
[8] Y. Naruse, N. Matsubara, *J. Micromech. Microeng.* **2009**, *19*, 1.
[9] F. Fan, Z. Tian, Z. L. Wang, *Nano Energy* **2012**, *1*, 328.
[10] S. Wang, L. Lin, Z. L. Wang, *Nano Lett.* **2012**, *12*, 6339.
[11] L. Lin, S. Wang, Y. Xie, Q. Jing, S. Niu, Y. Hu, Z. L. Wang, *Nano Lett.* **2013**, *13*, 2916.
[12] Y. Yang, Y. Zhou, H. Zhang, Y. Liu, *Adv. Mater.* **2013**, *25*, 6594.
[13] Z. L. Wang, *ACS Nano* **2013**, *7*, 9533.
[14] G. Zhu, J. Chen, T. Zhang, Q. Jing, Z. L. Wang, *Nat. Commun.* **2014**, *5*.
[15] G. Zhu, Y. Zhou, P. Bai, X. Meng, *Adv. Mater.* **2014**.
[16] S. Wang, Y. Xie, S. Niu, L. Lin, Z. Wang, *Adv. Mater.* **2014**, *26*, 2818.
[17] X. Zhang, M. Han, R. Wang, F. Zhu, Z. Li, W. Wang, H. X. Zhang, *Nano Lett.* **2013**, *13*, 1168.
[18] B. Meng, W. Tang, Z. Too, X. Zhang, M. Han, H. X. Zhang, *Energy Environ. Sci.* **2013**, *6*, 3235.
[19] W. Tang, B. Meng, H. X. Zhang, *Nano Energy* **2013**, *2*, 1164.
[20] P. Bai, G. Zhu, Y. Liu, J. Chen, Q. Jing, W. Yang, J. Ma, G. Zhang, Z. L. Wang, *ACS Nano* **2013**, *7*, 6361.
[21] S. Niu, S. Wang, Y. Liu, Y. Zhou, L. Lin, Y. Hu, K. C. Pradel, Z. L. Wang, *Energy Environ. Sci.* **2014**.
[22] C. Zhang, W. Tang, C. Han, F. Fan, Z. L. Wang, *Adv. Mater.* **2014**.
[23] X. S. Meng, G. Zhu, Z. L. Wang, *ACS Appl. Mater. Interfaces* **2014**, *6*, 8011.